ACS NANO

www.acsnano.org

ARTICLE

# Discriminating Residue Substitutions in a Single Protein Molecule Using a Sub-nanopore

Zhuxin Dong,[†] Eamonn Kennedy,[†] Mohammad Hokmabadi,[†] and Gregory Timp*[,‡]

[†]Department of Electrical Engineering and [‡]Departments of Electrical Engineering and Biological Science, University of Notre Dame, Notre Dame, Indiana 46556, United States

Supporting Information

**ABSTRACT:** It is now possible to create, in a thin inorganic membrane, a single, sub-nanometer-diameter pore (*i.e.*, a sub-nanopore) about the size of an amino acid residue. To explore the prospects for sequencing protein with it, measurements of the force and current were performed as two denatured histones, which differed by four amino acid residue substitutions, were impelled systematically through the sub-nanopore one at a time using an atomic force microscope. The force measurements revealed that once the denatured protein, stabilized by sodium dodecyl sulfate (SDS), translocated through the sub-nanopore, a disproportionately large force was required to pull it back. This was interpreted to mean that the SDS was cleaved from the protein during the translocation. The force measurements also exposed a dichotomy in the translocation kinetics: either the molecule slid nearly frictionlessly through the pore or it slipped-and-stuck. When it slid frictionlessly, regardless of whether the molecule was pulled N-terminus or C-terminus first through the pore, regular patterns were observed intermittently in the force and blockade current fluctuations that corresponded to the distance between stretched residues. Furthermore, the amplitude of the fluctuations in the current blockade were correlated with the occluded volume associated with the amino acid residues in the pore. Finally, a comparison of the patterns in the current fluctuations associated with the two practically identical histones supported the conclusion that a sub-nanopore was sensitive enough to discriminate amino acid substitutions in the sequence of *a single protein molecule* by measuring volumes of 0.1 nm$^3$ per read.

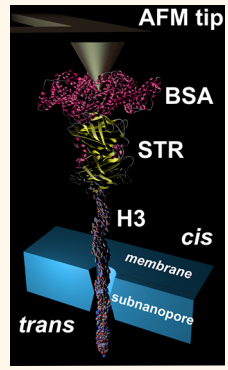


**KEYWORDS:** *protein sequencing, protein discrimination, sub-nanopore, single molecule spectroscopy, atomic force microscopy, protein denaturation*

Along with genomics and transcriptomics, systems biology is dictated by proteomics. Third generation, single-molecule sequencing of DNA and RNA, utilizing bleeding-edge technology such as a nanopore, has propelled genomics and transcriptomics through improved sensitivity and lower cost,[1−3] but proteomics has not benefited similarly mainly because amino acids (AAs) are so small and the structure of a whole protein is so complex. Currently, proteomics relies on a bottom-up approach to mass spectrometry (BU-MS). However, very few peptides of an intact protein can be detected unambiguously this way—isoforms (proteoforms) produced either from closely related duplicate genes or from the same gene by alternative splicing or by post-translational modifications (PTMs), proteolytic cleavage, or somatic recombination can go undetected.[4,5] Discriminating proteoforms with BU-MS requires the creation of a fragment ion library and matching unique fragment ions to entire proteins—a process that is frustrated by the enormous sequence homology shared by peptides. Thus, BU-MS does not inform on the complete sequence but rather identifies a limited number of protein fragments. On the other hand, top-down MS (TD-MS) identifies intact proteins and can be used to detect sequence variants or provide a scaffold for sequencing, but it lacks sensitivity—it is about 100-fold less sensitive than BU-MS; it is difficult and expensive to implement (requiring powerful magnets), and it has a room-sized footprint.[6] To sequence protein, what is needed is a tool with high sensitivity that can readily read the AA sequence of an intact, whole protein.

That is a tall order, however. The primary structure of a protein consists of a linear sequence of AAs linked by peptide bonds separated by about 0.38 nm (in equilibrium). Whereas 1 nm$^3$ of DNA contains a base pair, the volume of an AA is only about 0.1 nm$^3$ on average. Moreover, on average, about 485 AA residues comprise a human protein,[7,8] and so, several hundred reads that discriminate between subcubic nanometer volumes with sub-nanometer resolution are required for sequencing it. Recently, it has become possible to create a sub-nanopore in a thin, inorganic membrane about the size of an amino acid residue and with it read the primary structure of a protein.[9,10] In particular, the sequence of AA quadromers (four AA residues) in a denatured protein was read by measuring their volume.[9] The conditions for sequencing were hardly optimal, however. The mean read accuracy from a consensus of

Received: December 16, 2016
Accepted: May 24, 2017
Published: May 24, 2017






DOI: 10.1021/acsnano.6b08452
ACS Nano 2017, 11, 5440−5452

blockades was only 77% on average, and an improvement in the sensitivity was indicated as a consensus of hundreds of molecules was required to discriminate volumes >0.07 nm$^3$, comparable to the volume of the smallest AA, glycine, but still much larger than the difference between glycine and serine. Regardless, subsequent analysis using Random Forest regression, which reduced the errors associated with small volume reads and hydrophobicity, showed that it was still possible to discriminate a target protein ($p$ value $\sim 10^{-6}$) in a database covering 20% of the human proteome (14 293 proteins) with a cluster of only five blockades acquired from sub-nanopore measurements.[10] Thus, a sub-nanopore promises to extract the maximum amount of information about the primary structure of a protein from minimal material—a few or even one molecule.

With an eye toward improving the read accuracy, to inform on the physics underpinning a translocation, measurements of the force and current were performed as a single, denatured protein molecule was impelled systematically through a sub-nanopore with an atomic force microscope (AFM). To gauge the prospects for sequencing protein, two variants of the H3 histone (designated as H3.2 and H3.3) were analyzed this way. These histones were chosen because of their importance to epigenetics.[11] H3.2 and H3.3 consist of essentially the same chain of 136 AAs, differing only at positions 32, 88, 90, and 91 (see Supplemental Table S1), but nevertheless, they have distinctive expression patterns and chromatin incorporation mechanisms that turn out to be vital to biology. For example, there is the intriguing possibility that changes in the chromatin structure due to the replacement of H3.2 with H3.3 promote organismal aging through aberrant gene regulation in cells below the Hayflick limit.[12] Both H3.2 and H3.3 are also highly alkaline and positively charged, which is supposedly advantageous for sequencing as negatively charged AAs have produced read errors.[9] In addition, they are also larger than the peptides characterized by BU-MS. Thus, discriminating the AAs in these histones is an apt test of the sub-nanopore sensitivity.

## RESULTS AND DISCUSSION

The sub-nanopores were created by using a tightly focused electron beam in a scanning transmission electron microscope to sputter through a thin silicon nitride membrane nominally 10 nm thick, as described elsewhere.[9,13] The topography of a pore was inferred from TEM, but because the information limit of the microscope was 0.11 nm, for an accurate assessment, the TEM micrographs were imitated by multislice simulations (Figure 1a and supplemental Figure S1), which have also been described elsewhere.[9,14] The correspondence between the images (Figure 1a,i) and the simulations, which reproduced the actual imaging conditions (Figure 1a,ii), indicated that the models (Figure 1a,iii) were realistic representations of the actual pores. Thus, it was deduced that the pores were generally biconical, with cone angles that ranged around $\theta = 20 \pm 5°$, and irregular, with cross sections that were sub-nanometer in size along the major and minor axes at the waist ($0.5 \times 0.5$ nm$^2$ in Figure 1a). Pores ranging in cross section from $0.3 \times 0.3$ to $1.0 \times 1.7$ nm$^2$ were produced this way (supplemental Figure S1), but the results reported here mainly focus on five sub-nanopores with similar $0.20 \pm 0.06$ nm$^2$ cross sections.

An extension of finite element simulations (FESs) described elsewhere,[15] which accounted for the biconical pore topography (a 15° cone angle), the surface charge, the high viscosity of the fluid, and low ion mobility in a 0.5 nm diameter pore, but

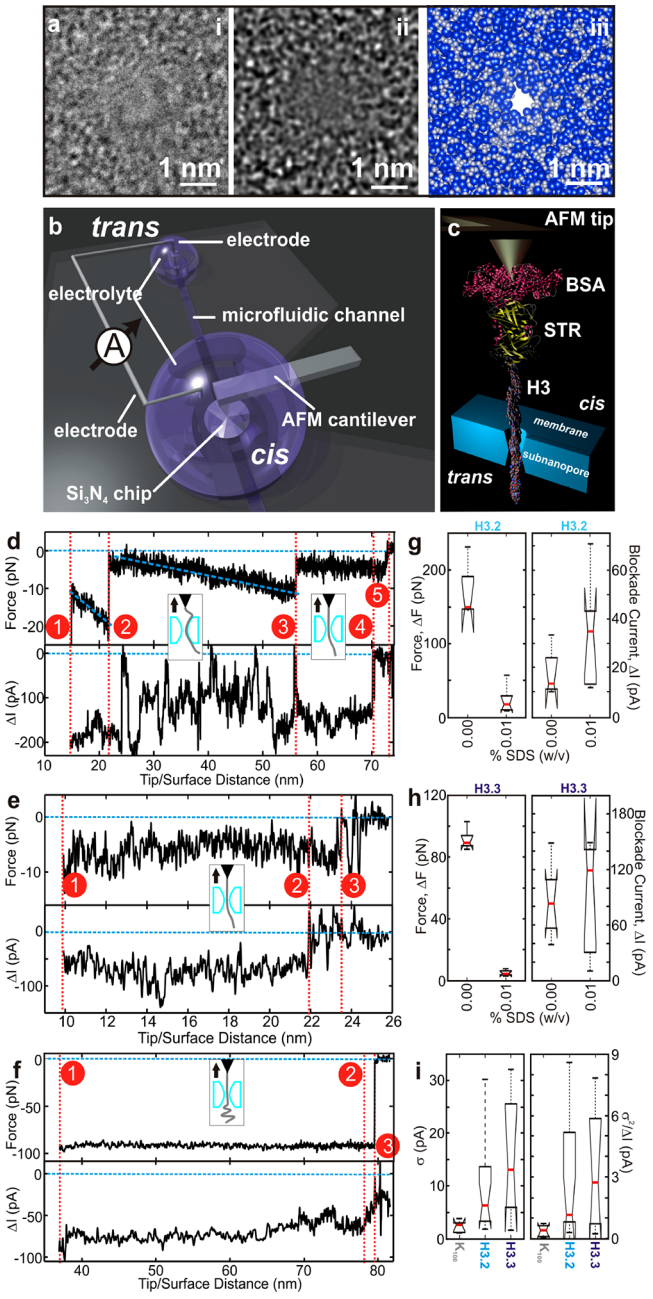


**Figure 1. Detecting single protein molecules using a sub-nanopore. (a,i) TEM micrograph of a sub-nanopore with a 0.5 nm diameter at the waist, sputtered through a silicon nitride membrane nominally 10 nm thick. The shot noise is associated with electron transmission through the pore. (a,ii) A multislice simulation consistent with the experimental conditions is shown. The simulation corresponds to biconical pores with a 20° cone angle at a defocus of 40 nm. The close correspondence between the simulation and the actual TEM image signified that the model accurately reflected the actual pore structure. (a,iii) Two-dimensional projection from the top through the model is shown that depicts the atomic distribution near the pore waist. The atoms are represented by a space-filling model in which *Si* is a sphere with a 0.235 nm diameter and *N* is a sphere with a 0.13 nm diameter. (b) Schematic representation is shown of the apparatus used to measure the force and current associated with a single protein translocating through a sub-nanopore. The sub-nanopore in a silicon nitride membrane was embedded in a two-layer (*cis*/*trans*) microfluidic device made from PDMS. An electrical bias of +0.70 V was applied between Ag/AgCl electrodes embedded in the *trans*-**



DOI: 10.1021/acsnano.6b08452
ACS Nano 2017, 11, 5440−5452

**Figure** 1. continued

**and *cis*-channels, respectively, and the current between them was measured using an amplifier. (c) Cutaway of the schematic showing a biotinylated H3 histone, tethered to the tip of an AFM cantilever through a bond to streptavidin (STR), translocating through the pore. (d–f) Concomitant direct measurements of the force and current as an H3.3 protein was impelled through the pore in (a) with 0.01% (w/v) SDS on the *trans*-side of the membrane (d,e) and without it (f). The force (top) on the protein and the blockade current (bottom) were measured with an applied potential of +0.70 V while the AFM cantilever was retracted from the pore at 4.00 nm/s, showing both slip-stick and a relatively frictionless plateau in the force. The dashed (blue) lines represent a fit to the FJC model for the stretches. On the other hand, the force plateaus (e,f) reflected a nearly frictionless translocation. Higher force was required to pull the histone through the pore in the absence of SDS on the *trans*-side (f). The dotted (cyan) lines offer guides for the eye. Insets: Cartoons show the assumed molecular configuration with the arrow indicating the direction of the cantilever motion. (g) Box-and-whisker plots are shown that summarize the distribution of force and current blockade measurements acquired from 14 H3.2, of which nine were done with SDS on the *trans*-side of the membrane and five without. (h) Like (g), but representing 10 H3.3 extractions, of which five were done with SDS on the *trans*-side and five without. (i) Box-and-whisker plots are shown that reflect the standard deviation ($\sigma$, left) and a normalized version ($\sigma_2/\sqrt{\Delta I}$, right) obtained from H3.2, H3.3, and $K_{100}$ molecules extracted from five pores about 0.20 ± 0.06 nm$^2$ in cross section.**

ignored the atomistic details of the structure and electrolyte, was used as a guide to discover the distribution of the electric field, forces, and current in the sub-nanopores. The simulations used a Poisson–Boltzmann formalism, which included the Navier–Stokes equation to account for the electro-osmotic flow; parameters such as mobility and viscosity were tightly constrained by values gleaned from the literature (see Methods). FES revealed that the electric field was tightly focused, peaking at 1.1 × 10$^6$ V/cm near the center of the membrane for a 0.70 V bias and decaying to 6 × 10$^4$ V/cm about 10 nm above the opening.[9,15] Thus, it was likely that the electric force due to the field above the membrane facilitated the capture and delayed the release of the molecule from the pore. According to this reckoning (see Methods), the force on a single protein–SDS aggregate was mainly due to the electrophoretic component (14 pN), since the electro-osmotic component was much smaller (4 pN).[15] The simulations also captured the measured current–voltage characteristics, although the ion mobility (fluid viscosity) was generally much smaller (larger) than the corresponding bulk values (supplemental Figure S2 and Table S2). Finally, these facts seem to corroborate the idea that sub-nanopores with this topography crowd the ionic current near the waist into a region about 1.5 nm in extent along the pore axis, increasing the sensitivity there.[9]

AFM was the linchpin supporting the single molecule measurements. To systematically impel a single molecule through a sub-nanopore, biotinylated protein was first denatured by heat, stabilized with sodium dodecyl sulfate (SDS) and $\beta$-mercaptoethanol (BME), and then the protein–SDS aggregate was tethered to the tip of an AFM cantilever with a soft spring constant using streptavidin (STR) and bovine serum albumin (BSA) (see Methods). Native histones have a characteristic fold consisting of $\alpha$-helices (which have a diameter of about 1.2 nm). Whereas the mean residual ellipticity in circular dichroism (CD) spectra of the native protein, measured in the UV range (195–260 nm), produced a broad negative peak from 205 to 235 nm, which was identified with two signature peaks near 208 and 222 nm that are characteristic of an $\alpha$-helix, this signature was absent in the CD spectra after denaturation, indicating that the secondary structure of the histones remained unfolded after denaturation (see Methods and supplemental Figure S3). Although the exact structure of the denatured protein–SDS aggregate remains unsolved, a "rod-like" model was adopted here in which the SDS molecules formed a uniformly charged shell along the length of the protein backbone.[16,17]

The denatured, tethered aggregate was advanced by the AFM toward the sub-nanopore, captured, and threaded through it by the electric field and then retracted from it at a constant velocity, while the tip deflection and current were recorded (Figures 1b,c) to measure the force and blockade current. Experiments configured this way offered the advantage of systematic control of the translocation kinetics, but that was offset by a 2-fold noisier current measurement, even inside a Faraday cage (see Methods). Whereas the duration of the translocation for an *untethered* molecule ranged from 0.5 to 1.0 ms, corresponding to an average velocity of about 3 × 10$^4$ nm/s (10$^5$ residues/s), the retraction velocity in these experiments was typically 4 nm/s (10 residues/s), which translated to a single molecule trapped for 10–20 s in the pore. The 10000-fold reduction in translocation velocity offered the prospect of improving the signal-to-noise ratio through signal averaging, which more than offset the increased electrical noise.

With a +0.70 V bias applied constantly between the *trans*- and *cis*-channels, the force on the protein–SDS aggregate and current through the pore were recorded as the tip was advanced toward and retracted from the membrane. Occasionally, first the force and then later the current measurements reflected the capture, translocation, and subsequent evacuation of the molecule from the pore (Figure 1d–f). The blockade of the electrolytic current through the pore, associated with the occluded volume near the waist, provided an unambiguous signature of the protein–SDS aggregate trapped there. Due to its size (288.4 Da), it seemed likely that the SDS was cleaved from the protein by the steric constraints imposed by the sub-nanopore topography above the waist during the translocation. So, to stabilize the denatured protein (see Methods), the 250 mM NaCl electrolyte on both sides of the membrane contained a superfluous amount of SDS (0.01% w/v). This concentration was determined by the retraction velocity through the sub-nanopore and the time required for SDS to diffuse to the protein.

Based on empirical evidence, it has been argued that the fractional change in the blockade current, $\Delta I/I_0$, scales like the ratio of the occluded molecular volume to the pore volume according to $\Delta I/I_0 = f\Delta V_{mol}/V_{pore}S$, where $f$ is a gauge of the molecular shape and orientation and $S$ is a size factor that accounts for distortions in the electric field that occur when the molecule is comparable in size to the pore.[18,19] This notion is doubtlessly naïve in a sub-nanopore with a waist that is not only comparable in size to an AA but also a hydrated ion. With this proviso, a crude estimate of blockade current associated with a single protein molecule can be extracted. Accordingly, using a sub-nanopore topography, but ignoring the size factor, if the denatured histone had a rod-like shape and the distance between AAs was about 0.38 nm, then 26 AAs would span a membrane 10 nm thick, and so, $\Delta V_{26AA}/V_{pore}$ = 4.16 nm$^3$/31.3



DOI: 10.1021/acsnano.6b08452
*ACS Nano* 2017, 11, 5440–5452

$nm^3 = 0.109 \propto \Delta I/I_0$ or $\Delta I \geq 20$ pA for $I_0 = 200$ pA. On the other hand, if current crowding associated with the biconical topography essentially determines the blockade, then only four AAs would span a thickness of 1.5 nm, and so $\Delta V_{4AA}/V_{pore}^{eff} = 0.44\ nm^3/0.59\ nm^3 = 0.75 \propto \Delta I/I_0$, producing a blockade of about $\Delta I = 150$ pA. Thus, a blockade in the range 20 pA $\leq \Delta I \leq$ 150 pA acted as a signature of a single molecule trapped in the sub-nanopore.

When the blockade current indicated a molecule was trapped, the force measurements exposed a dichotomy in the translocation kinetics through a sub-nanopore; either the protein slipped-and-stuck to the membrane and/or it slid nearly frictionlessly through the pore. For example, force measurements performed on a single H3.3 molecule as the cantilever was retracted from a 0.5 nm diameter pore at a constant velocity of 4.00 ± 0.02 nm/s against a potential of 0.70 V revealed *both* slip-stick and frictionless kinetics consecutively (Figure 1d). As it retracted from the sub-nanopore, the adhesion between the tip and the membrane predominated for separations <15 nm. However, when the tip was released from the surface at position (1), a force of 11 ± 1 pN was measured on the molecule, whereas the blockade current of $\Delta I = 205 \pm 5$ pA indicated a molecular volume larger than that ascribed to a single linear chain of AAs spanning the membrane. The protein was subsequently stretched by the differential force $\Delta F = 8.3$ pN over a distance of 6.6 nm until the bond ruptured at position (2). Likewise, between positions (2) and (3), the protein was stretched again by a differential force $\Delta F = 10$ pN over 34.2 nm until the bond ruptured at position (3).

Any time the translocation kinetics through a pore resembled a "slip-stick" motion, it was assumed that the polymer rapidly slipped as soon as the applied force exceeded the threshold for rupturing the adhesive bond between the aggregate and the membrane. According to this interpretation, the excessive blockade current may then be attributed to contortions in the conformation of the protein−SDS aggregate near the pore waist. Usually, a force−extension curve like this reflects the elasticity of the molecule. Stretching events like these can be described by statistical mechanical polymer elasticity models, of which the most commonly used are the freely jointed chain (FJC) model[20] or the worm-like chain model.[21] Using the FJC, with a Kuhn length of $b \sim 0.3$−0.4 nm,[22] the effective spring constant associated with each stretching event was estimated from $K_{eff} = 3k_BT/bX$, where $k_BT$ represents the thermal energy at 293 K and $X$ is the extension of the protein relative to its total length to find $K_{eff} = 2.1 \pm 0.9$ pN/nm, which is consistent with prior estimates.[23−25] At a constant retraction velocity of 4 nm/s, this spring constant implies a loading rate of 8.4 pN/s, indicating a near-equilibrium loading regime and a single bond type.

On the other hand, from position (3) at a tip-to-surface distance of about 56 nm, the protein slid relatively frictionlessly at a force of $\Delta F = 5 \pm 1$ pN over a distance of about 14.3 nm until the current returned to the open pore value and the molecule vacated the pore waist near position (4). Eventually, when it retracted 2.7 nm further and cleared the membrane at position (5), the data were interpreted to show that the electric force on the molecule became negligible, too. Frictionless kinetics were observed without a slip-and-stick motion, as well. For example, in Figure 1e, from position (1) at a tip-to-surface distance of about 10 nm, a single H3.3 molecule, producing a $\Delta I = 70 \pm 20$ pA blockade in the pore current, was observed to slide relatively frictionlessly at a force of $\Delta F = 6 \pm 2$ pN over a distance of about 12.0 nm until the current recovered to the open pore value near position (2), where the molecule vacated the pore waist. Eventually, after retracting an additional 1.5 nm to position (3), the load on the molecule was also relieved. Thus, after the molecule was forced through a sub-nanopore from the *cis*- to the *trans*-side of the membrane, only a small force was required to pull it back to the *cis*-side, which supports a "rod-like" model for the structure of the protein−SDS aggregate.

Force plateaus like these were reminiscent of observations made when single-stranded DNA (ssDNA) was impelled through a 1 nm diameter pore through a silicon nitride membrane or pulled off a surface.[15] Since the protein−SDS aggregate has some properties that are similar to ssDNA, such as regularly spaced negative charges and aromatic rings, it was reasoned that the translocation kinetics and transport properties should be similar, too, as suggested by simulations of a protein translocating through a nanopore.[26] On the other hand, constant force plateaus like those in Figure 1d−f were also observed without the protein in the pore (in the absence of a current blockade) as the molecule was peeled from the surface of the membrane (supplemental Figure S4). A protein sliding frictionlessly, either along a surface or through a pore, has not been reported previously—probably because prior work had focused on unraveling native protein tethered to an AFM cantilever and bound to a surface to inform on how a native protein unfolds, instead of denatured protein−SDS aggregates.

Measurements of the force support the assertion that SDS was cleaved from the protein during the translocation through a sub-nanopore. Force measurements performed on the same protein translocating through the same sub-nanopore (0.5 nm diameter) under the same conditions, but *with* and *without* any SDS intentionally in solution on the *trans*-side of the membrane, were disproportionately affected (Figure 1e,f and supplemental Figures S5 and S6). *Without* SDS, in contrast with data shown in Figure 1e, as the tip was retracted from the pore and released from the surface at position (1), a larger force, $\Delta F = 93 \pm 5$ pN, was required to extract the H3.3 molecule from the pore, whereas the corresponding blockade current, $\Delta I = 80 \pm 5$ pA, remained about the same (Figure 1f). Subsequently, the protein translocated through the pore with only miniscule changes in the force over a distance of about 41 nm until, at position (2), the current returned to the open pore value, indicating that the molecule vacated the pore there. Finally, when position (3) was reached, after an additional retraction of 1.3 nm, the load on the molecule was relieved.

These same trends in the force and blockade current were observed repeatedly, in data comprising 24 concurrent measurements of the force and current acquired from five sub-nanopores; that is, larger forces were required to pull a single molecule through a sub-nanopore in the absence of SDS on the *trans*-side of the membrane (Figure 1g,h). To calculate the median force, traces like those in Figure 1d−f were cropped to regions over which the blockade could be attributed to a frictionless translocation. Thus, the median force to pull H3.2 through a sub-nanopore *with* SDS on the *trans*-side was only 18 pN, whereas it increased to 150 pN without it (Figure 1g). Likewise, the median force to pull H3.3 through a sub-nanopore *with* (*without*) SDS on the *trans*-side of the membrane was 4.4 (89.3) pN (Figure 1h). The $p$ values = $5.3 \times 10^{-5}$ ($3.6 \times 10^{-9}$), which were associated with the distributions *with* and *without* SDS for H3.2 (H3.3), indicated



DOI: 10.1021/acsnano.6b08452
ACS Nano 2017, 11, 5440−5452

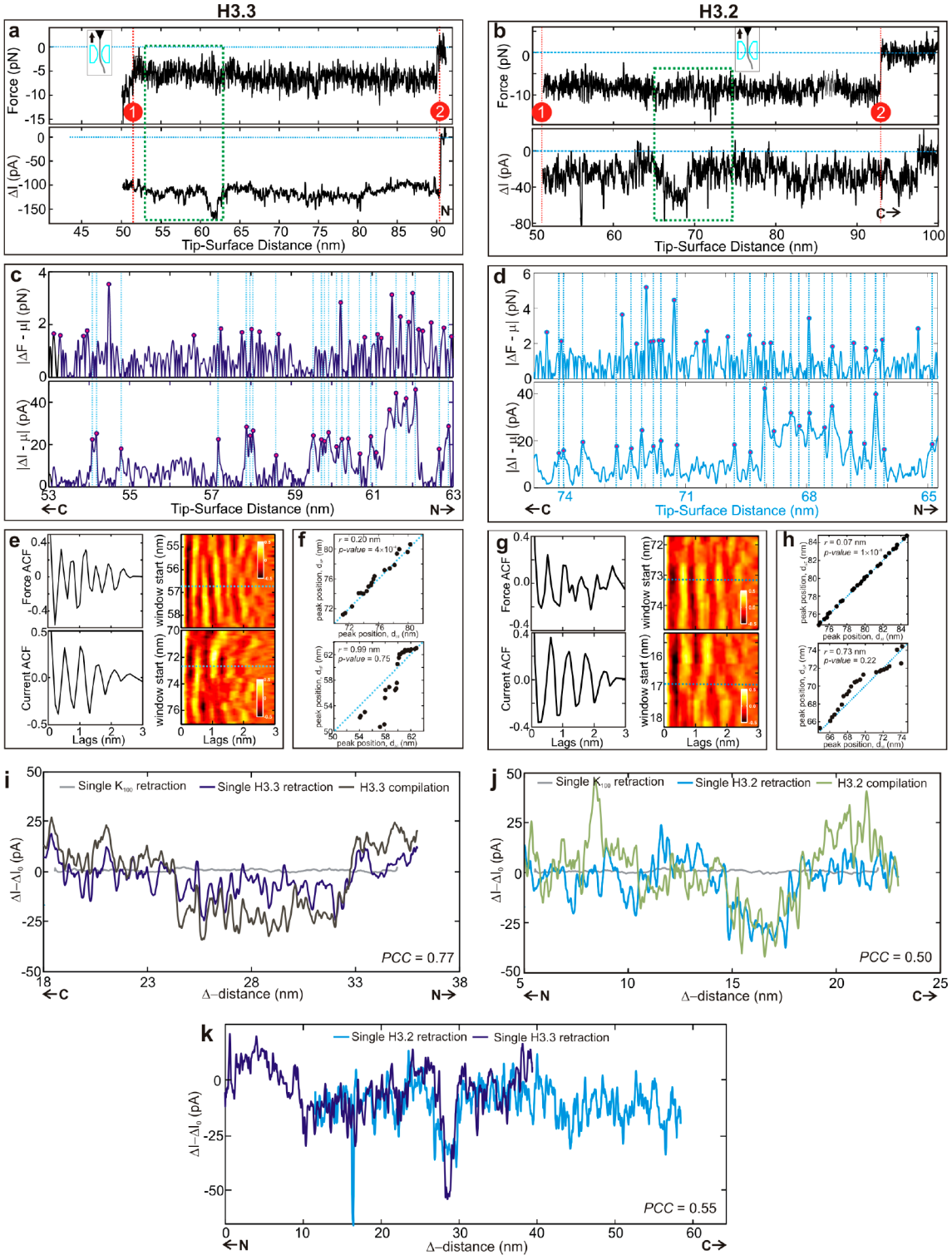


**Figure 2. Forces and currents measured as a single histone, either H3.3 or H3.2, was impelled through a sub-nanopore. (a,b) Force (top) and blockade current (bottom) measured as a single H3.3 or H3.2, respectively, was extracted at 4.0 nm/s from a 0.5 nm diameter sub-nanopore against a potential of +0.70 V, applied between *trans*- and *cis*-channels. H3.2 was impelled from the N- to the C-terminus, whereas H3.3 was just the opposite. The C- and N-termini are indicated along the abscissas. The cartoons show the assumed molecular configuration with the arrow indicating the direction of the cantilever motion. The dotted (cyan) lines offer guides for the eye. (c,d) Like (a,b), but a magnified view of the regions highlighted by green dotted boxes in (a,b), which show the magnitudes of the same force (top) and blockade current (bottom) data after subtracting the mean ($\mu$) over a select region and illustrate fluctuating patterns in the force and current. The circles denote the fluctuations above the noise identified in the blockade current using a $2\sigma$ criterion. The (blue) vertical lines are used to facilitate the comparison of the alignment of the force fluctuations relative to the current fluctuations. For comparison to (d), the abscissa in (c) is reversed to reflect that H3.2 was pulled through the pore N-terminus first. The direction of the C- and N-termini are indicated along the abscissas. (e, Left) Corresponding ACFs of the force (top) and current (bottom) for H3.3 are shown of the traces highlighted by the dotted (cyan) lines in (e, right). (e, Right) Kymographs of the force (top) and current (bottom) are shown that represent a compilation of ACFs similar to (e, left)**



DOI: 10.1021/acsnano.6b08452
*ACS Nano* 2017, 11, 5440−5452

**Figure** 2. continued

**obtained with a 3 nm window but with a start staggered by 0.1 nm. (f) Top (bottom) plots depict the cross-correlation between the positions of the force and current fluctuations for H3.3 in (a). (g, Left) Like (e, left) but for H3.2. (g, Right) Like (e, right), but for H3.2. (h) Like (f), but for H3.2, depicting the cross-correlation between the positions of the force and current fluctuations in (b). (i,j) These figures juxtapose single extractions taken from (a,b) with aligned compilations comprising six and five retractions of H3.3 and H3.2 molecules, respectively. The single extractions for H3.3 and H3.2 were well correlated to the respective compilations according to PCC = 0.77 and 0.50. The directions of the C- and N-termini are indicated along the abscissas. (k) Accounting for the different orientations of H3.3 and H3.2, this figure juxtaposes the blockade data of (a,b), illustrating correlated features in the region where they overlap (PCC = 0.55).**

that it was highly unlikely that the median from one distribution could be considered as an extremity of the other. On the other hand, irrespective of the SDS concentration on the *trans*-side of the membrane, even though the median increased 2-fold with SDS from 14 to 35 pA for H3.2 and 84 to 120 pA for H3.3, the change in blockade current was not statistically significant as evident from the overlap in the extent of the boxes. (The respective $p$ values were 0.23 and 0.88 for H3.2 and H3.3.)

Taken altogether, these data were interpreted as evidence that the SDS was cleaved from the protein as the aggregate was impelled through the sub-nanopore from the *cis*-side. It was asserted that, absent SDS to maintain denaturation on the *trans*-side of the membrane, the protein refolded so that more force was required to unfold and retract the protein through the pore. On the other hand, replenished from a high concentration of SDS in solution on the *trans*-side of the membrane, if denaturation was maintained and the protein did not refold, then force required for retraction was minimal. This assertion was also consistent with the idea that the blockade current was essentially determined by the occluded volume of an undecorated protein in the pore waist as the change in the blockade *with* and *without* SDS was statistically insignificant. Interestingly, frictionless translocations of a denatured protein through pores with $a > 1$ nm diameter consistently required a larger ($\Delta F > 100$ pN) force (supplemental Figure S7) regardless of the concentration of SDS on the *trans*-side of the membrane, in contrast to the results obtained from sub-nanopores, which we attributed to a size limitation for cleavage. Apparently, SDS binds the protein throughout a translocation through a 1 nm diameter pore, which results in large mechanical force requirement due to the large electrical force on the charged protein−SDS aggregate.

Parenthetically, two biotinylated homopolymers, poly-L-lysine (denoted as $K_{100}$) and poly-L-glutamic acid ($E_{200}$), which were used as controls, presented additional curiosities regarding the cleavage of SDS (see supplemental Figures S8 and S9). The homopolymer, $K_{100}$, is positively charged so that negatively charged SDS should readily bind to it, whereas $E_{200}$ is negatively charged so that binding to SDS may be more problematic. A large force was usually required to pull $E_{200}$ through a sub-nanopore but not always (supplemental Figure S8), whereas $K_{100}$ offered little resistance to translocation (supplemental Figure S9). These data were interpreted to mean that the presumed rod-like structure of negatively charged SDS-$E_{200}$ aggregate was unstable, even with superfluous SDS, and reverted to a remnant native form, whereas the SDS binds to positively charged $K_{100}$ as per usual. Thus, it was reasoned that a remnant native structure, which developed in the absence of SDS, contributed to the force required to impel a single protein molecule through a sub-nanopore, the magnitude of which was consistent with other measurements of the force required to mechanically unfold protein.[24,25]

Besides the dependence on SDS, the evidence also indicated that the force and the blockade current were affected by how the molecule was oriented in the pore relative to the pulling force. The biotin tag on H3.2 was on the N-terminus and likewise for the $K_{100}$ control, whereas the C-terminus was biotinylated on H3.3. Coincidently, it was observed that, *with* SDS on the *trans*-side, the median force required to pull H3.2 through a sub-nanopore was consistently larger (18 pN > 4.4 pN), and the resulting median blockade current was smaller (35 pA < 120 pA) measured relative to H3.3 (and yet comparable to the control since $\Delta F_{K100} = 9.6$ pN and $\Delta I_{K100} = 18.7$ pA). The larger force likely caused the H3.2 molecule to stretch more than H3.3, which diminished the blockade current due to the reduced volume. If this difference is probative, then it demonstrated a so-called "Christmas-tree effect" in which the AA side chains tilted preferentially away from the backbone toward the N-terminus, like the branches of an ever-green tree. A similar directionality has been seen before in electron density maps of protein.[27]

These results were typical. In a data set of 125 force curves measured with SDS on the *trans*-side of the membrane, there were only 10 events in which the current and the force were affected concurrently, of which seven "slip-stick" force curves were observed and three were considered nearly frictionless. Several interesting features were distilled from the analysis of the subset of data for which the translocations were nearly frictionless. In particular, a statistical analysis of the variance (ANOVA) of the force and blockade current from the ensemble of data acquired from all the sub-nanopores used in this work exposed fluctuations above the estimated minimum noise that persisted even after repeated cycles of insertion and retraction through the same pore (supplemental Figure S10). Using either the standard deviation, $\sigma$, or more accurately the fluctuation strength, defined by the quantity $\sigma^2/\langle\Delta I\rangle$ that decreases as the mean increases, to gauge the amplitude of fluctuations within a blockade, a salient feature was discovered in the data; that is, the fluctuation strength for the homopolymer control was minute ($\sigma^2_{K_{100}}/\langle\Delta I_{K_{100}}\rangle = 0.13$) in comparison to either histone ($\sigma^2_{H3.2}/\langle\Delta I_{H3.2}\rangle = 5.3$; $\sigma^2_{H3.3}/\langle\Delta I_{H3.3}\rangle = 4.8$) (Figure 1i, right). As the fluctuations were more pronounced in the heteropolymers (histones), it was argued that the fluctuations in the blockade current informed on the variation of the AA volumes constituting the occluded volume in the waist.

Beyond statistical inference, close scrutiny revealed aspects of the data that supported this argument in detail. Although the data shown in Figure 2 were exceptional, they were especially illuminating because they spanned nearly the entire H3.2 and H3.3 sequences. (Traces like those shown in Figures S5−11 were typical.) When H3.3 was pulled systematically at a constant velocity of 4.00 ± 0.01 nm/s against 0.70 V through a 0.5 nm diameter pore, the molecule was observed to slide nearly frictionlessly from position (1), where a force of $\Delta F = 5$



DOI: 10.1021/acsnano.6b08452
*ACS Nano* 2017, 11, 5440−5452

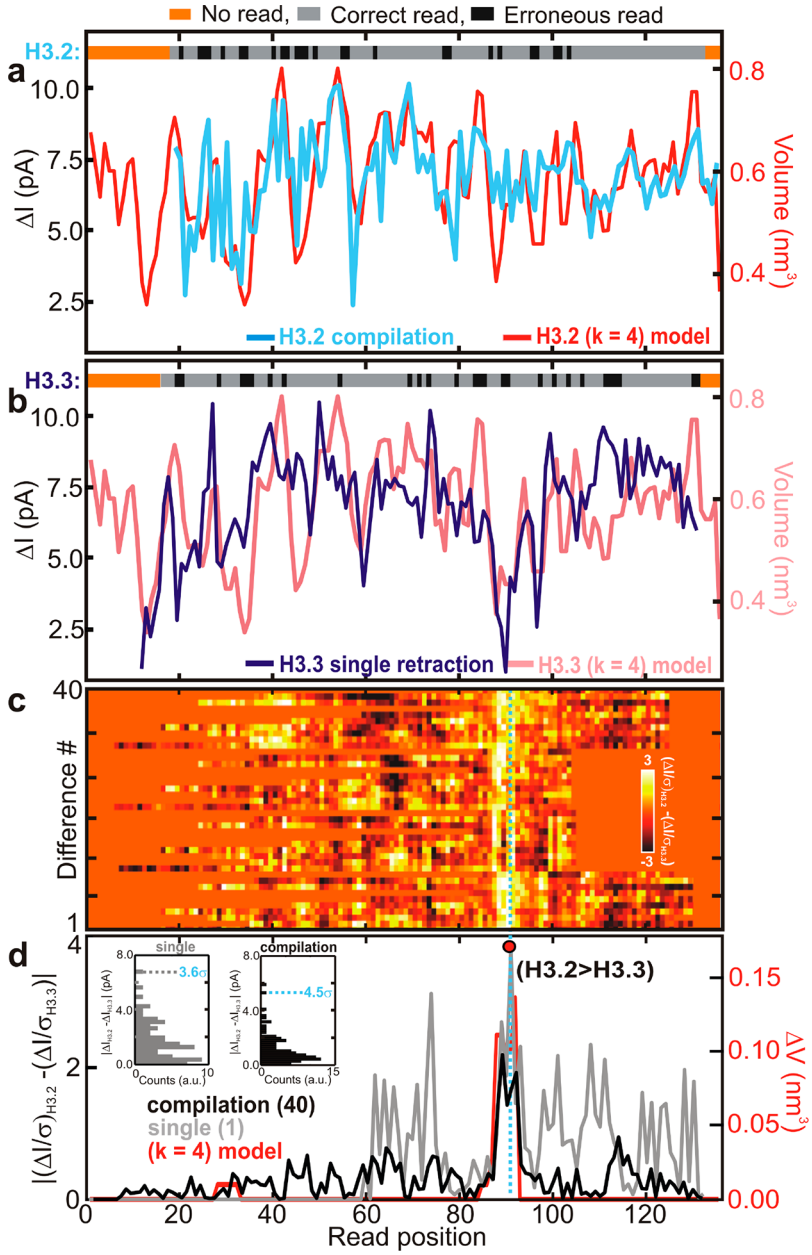


**Figure 3. Protein sequence analysis. (a, Top) Quadromer error map is shown that indicates the read fidelity for a compilation of the H3.2 variant. The positions where the empirical reads shown in (a, bottom) are correct (incorrect) are represented in gray (black), whereas no read at all is represented in orange. (a, Bottom) Figure juxtaposes for comparison a compilation of 10 blockade currents associated with the retraction of a single H3.2 molecule (light blue) frictionlessly from a 0.5 nm diameter sub-nanopore with a +0.70 V bias applied between the *trans*- and *cis*-channels, respectively, with a volume model (red). The AA volume model for the H3.3 variant assumes that $k = 4$. (b) Like (a), the figure shows (top) a quadromer error map and (bottom) a juxtaposition of the blockade current but associated with a single H3.3 molecule (dark blue) acquired under the same conditions from the same sub-nanopore with a volume model (red). (c) Heat map is shown that conveys 40 signed differences of H3.2 and H3.3 blockades. Where no overlap information was available, the molecules were assumed to have the same volume. A salient feature associated with a larger quadromer volume in H3.2 was repeatedly observed near read position 90 compared to H3.3. (d) Magnitude of the differences between a single H3.2 and H3.3 retractions (gray) and compilations of 40 differences (black) are shown, along with the difference between the corresponding volume models (red) plotted in units of nm³ (right ordinate). According to the volume model, the H3.2 trace overlaps the H3.3 trace except near the read positions 32, 88, 90, and 91, where AA substitutions occur. (Inset, right) Histogram is shown that relates the frequency of the difference measured for the compilation in (d), indicating that the peak observed near read position 90 is 4.5 $\sigma$ above the baseline. (Inset, left) Histogram is shown that relates the frequency of the difference measured for the single blockade in (d), indicating that the peak observed near read position 90 is 3.6 $\sigma$ above the baseline.**

± 2 pN was measured, corresponding with a blockade current of $\Delta I$ = 105 ± 7 pA until it reached position (2), where it vacated the pore waist and subsequently the force was relieved (Figure 2a). Likewise, when H3.2 was pulled systematically through a similar 0.5 nm diameter pore under the same conditions, the molecule was observed to slide nearly frictionlessly from position (1), requiring a force of $\Delta F$ = 7 ± 2 pN, corresponding with a blockade current of $\Delta I$ = 21 ± 8 pA, to position (2) where the force was relieved, likely because the tether ruptured there (Figure 2b). Because the translocation



DOI: 10.1021/acsnano.6b08452
ACS Nano 2017, 11, 5440−5452

velocity of these molecules were relatively constant between positions (1) and (2), assuming a distance between AAs ≥ 0.38 nm, it was inferred that at least 80 AAs were observed translocating through the pore in these two cases (similar data were acquired for H3.3 and H3.2 *with* and *without* SDS on the *trans*-side of the membrane; see supplemental Figures S5, S6, and S11 and supplementary note #1).

Coinciding with this estimate, magnified views of the force and blockade exposed fluctuations that tallied 75(78) within the 39(41) nm range of the current blockade for H3.3 (H3.2), indicating an average interval of about 0.52(0.53) nm between them (Figure 2c,d). Moreover, the fluctuations were observed intermittently to be nearly regular, as was apparent in the corresponding autocorrelation functions (ACFs) of the same data (Figure 2e,g, left), which indicated force oscillations with a mean lag of 0.40 ± 0.05 nm (0.52 ± 0.03 nm) for H3.3 (H3.2), and likewise at the same tip-to-surface height, current oscillations were observed with a mean lag of 0.50 ± 0.06 nm (0.54 ± 0.10 nm) for H3.3 (H3.2). These values either equaled or exceeded the equilibrium distance between residues (0.38 nm), indicating that the molecules were likely stretched. The separation between peaks in the force and current ACF were nearly equidistant over only a limited range, however, as evident in the kymographs (Figures 2e,g, right), which represent a compilation of ACFs using a 3.0 nm wide moving window with a starting position that was staggered by 0.1 nm.

Since both the force and current fluctuations were consistent with the separation between residues, it was argued that each fluctuation in the blockade current reflected an event in which one AA entered the pore while another left, which occurred about every 0.4−0.55 nm.[9] The irregularities or displacements from a regular pattern (*i.e.*, the "jitter" in the fluctuations) were attributed to the different mobilities associated with different sized residues in the sub-nanopore and/or nonspecific binding to the membrane. Because it was likely that counterions moved along with a protein−SDS aggregate to minimize Coulomb repulsion, and since a sub-nanopore has a diameter comparable to a residue, the motion of the ensemble through it would be impeded by steric hindrances. Thus, the fluctuating patterns were generally consistent with a halting, turnstile motion in which the AAs stalled repeatedly within the pore and then eventually proceeded through it due to the force applied by the AFM.[9] This turnstile-type of motion was again reminiscent of observations made when ssDNA was forced through a 1 nm diameter pore by an AFM.[15]

Frequently the fluctuations in the force and current were cross-correlated, although imperfectly, likely due to the minimum force noise that was ∼1 pN (see Methods). After normalizing by subtracting the mean ($\mu$), the average force-to-current positional difference ($r$) was used to gauge the linear correlation between the positions of the fluctuations in the force and the current blockade (Figure 2f,h) for H3.3 and H3.2, respectively. Choosing a threshold of twice the standard deviation, $2\sigma$ (*i.e.*, $|\Delta X - \mu(X)| > 2\sigma$), it was determined that $r$ = 0.20 nm (0.07 nm) over the range from 70 to 82 nm (75 to 85 nm) with corresponding $p$ values $<4 \times 10^{-4}$ ($10^{-8}$) for H3.3 (H3.2) with respect to random peak placements (Figure 2f,h, top). These $p$ values indicated that, with >99% confidence, the peaks in the force and blockade current were anomalously cross-correlated compared to stochastically positioned peaks within these ranges. However, the $p$ values inferred from the data over the range in Figure 2c,d (see Figure 2f,h, bottom) showed that the force fluctuations for H3.3 (H3.2) were not always so well correlated with the current fluctuations (*e.g.*, $r$ = 0.99 (0.73) nm with $p$ values = 0.75(0.56)), which may be attributed to force noise.

On the other hand, the current fluctuations acquired from different pores using the same histone or even different histones were highly correlated (Figure 2i,j) to each other, proving the similarity of the data. For example, the Pearson correlation coefficient (PCC) between a single retraction of H3.3(H3.2) and six(five) aligned compilations of H3.3(H3.2) retractions indicated PCC = 0.77(0.50) over 18 nm. Finally, the H3.2 current blockades were conspicuously mirrored in the H3.3 measurements because the biotin tags were on the opposite termini (Figure 2c,d). The PCC = 0.55 between the 27.4 nm region over which a single H3.2 retraction overlapped with a single H3.3 retraction demonstrated the similarity of the two different histones (Figure 2k). To reinforce the argument that these fluctuations informed on the AA sequence of the histones, a comparison with a homopolymer ($K_{100}$) control is offered in Figure 2i,j (gray). The blockades associated with a single $K_{100}$ retracted systematically through a similar sub-nanopore, measured under the same conditions over the same distance, produced much smaller fluctuation amplitudes, consistent with the fluctuation strength reported in Figure 1i, from which it was inferred that the AA volume was practically uniform along the peptide chain.

Subsequently, the assertion that the current fluctuations informed on the AA sequence was rigorously tested by correlating the fluctuations in the blockade current to a naïve model for the protein in which each AA was represented by its volume estimated from crystallography data (Figure 3a,b).[28,29] As in prior work,[9] to account for the current crowding, the model employed a moving average performed on the sequence of volumes with a window size ($k$ = 4) corresponding to about four AAs spanning the 1.5 nm thick waist (*i.e.*, a quadromer). The results show that the volume model was well correlated with single retractions of H3.2(H3.3) as PCC = 0.42(0.47), whereas PCC = 0.61(0.40) for the compilations of extractions that spanned entire molecules. The correlations to the volume model obtained from single blockades of tethered molecules were superior, on average, to that obtained from single blockades in pores with a similar cross section without a tethered (supplemental note 2 and Figure S12).[9,10] Interestingly, decreasing the pore cross section to 0.20 nm$^2$ also improved the correlation between a single extraction spanning 50 to 70 AAs and the model to PCC = 0.45, on average, from the lower extreme (PCC = 0.10) associated with pores >1.0 nm$^2$ in cross section (see supplemental Figure S7).

The correlation between the data acquired from pores with 0.20 nm$^2$ cross section and the volume model corresponds to a mean read accuracy of 72% with a 20% threshold tolerance. The quadromer error maps (Figure 3a,b, top) reflect the agreement between the empirical data acquired from the compilation and the $k$ = 4 model in which each correct (erroneous) read is expressed as gray (black) calls, depending on whether the agreement was greater (or less) than 20%. Since each read reflected the optimally ranged occluded volume associated with multiple AA residues in the pore waist, the accuracy was defined by the difference between the measured and model volumes. The threshold tolerance for an accurate read was chosen to be 20%, which means that, on average, ±20% of optimally ranged and fitted random noise would fit the model because 40% of all data will fall within its threshold−tolerance boundary. Thus, from this significance level, it was



DOI: 10.1021/acsnano.6b08452
*ACS Nano* 2017, 11, 5440−5452

inferred that each fluctuation represented a (low) fidelity read, measuring the occluded volume associated with a quadromer in the histones. This inference was also consistent with force and blockade current measurements performed on the controls. As the controls were homopolymers, no fluctuation in the amplitude was expected across a blockade (except near the protein terminus) or observed outside the noise.

Although the volume model accounted for the empirical data, it was nevertheless naïve because it ignored physical properties such as hydrophilicity that were proven predictors.[10] However, striking differences that were observed repeatedly between the variants could be attributed to residue substitutions, *without reference to any model*. To elucidate the differences, blockades for the two histones were first zeroed and then normalized by their respective standard deviations to produce $(\Delta I - \langle \Delta I \rangle)/\sigma_{\Delta I}$ prior to subtraction (Figure 3c,d). A peak in the magnitude of the difference between the two variants occurred near read position 90 with a $2-\sigma$ to $3.6-\sigma$ significance, depending on the blockades forming the difference, which coincided with substitutions in the sequences near there. The empirical data repeatedly peaked in the range between position 89 and position 92, showing consistently a larger H3.2 volume there (Figure 3c,d and supplemental Figure S12). Averaging (over 40 differences) pushed the confidence level of the H3.2 to H3.3 difference near position 90 to $4.5-\sigma$ relative to background fluctuations. Moreover, the same discrepancy between the variants was also found without systematic control of the velocity, but with less $(1.6-\sigma)$ confidence (supplemental Figure S12).

The peaks in the difference near position 90 were attributed to the occluded volume differences associated with the substitutions in the AA sequences there, which were supposed to occur at positions 88, 90, and 91. For H3.2, at positions 88–91, the sequence was supposed to be SAVM, whereas it was AAIG for H3.3. All of these substitutions doubtlessly contribute to the empirical reads, but it was reasoned that the M → G substitution at position 91, which is associated with the largest volume change, $\Delta V_{mol} = 0.104$ nm$^3$, accounted for at least 71% of the total volume difference. The corresponding differences between the quadromer reads of the volume models for H3.2 and H3.3 indicated a peak in volume near a read position of 91, irrespective of the size of the window, $k$ (red line in Figure 3d). Any discrepancies between the empirical position of the peak and the model were attributed to the error associated with the detection of the protein terminus within the pore waist. The best fit to the model deviated 1.44 AA positions (on average). Accordingly, if the difference between the H3.2 and H3.3 data near read position 90 was assigned to a quadromer read at position 91, then a lower bound on the sensitivity would be about 0.1 nm$^3$. Thus, regardless of the model, residue substitutions in molecular variants of *single histone molecules* could be discriminated by reading their difference, which reflected the extraordinary sensitivity of a sub-nanopore. Finally, there was supposed to be an A → S substitution between H3.2 and H3.3 at position 32, but the corresponding change in the residue volume $\Delta V_{mol} = 0.0076$ nm$^3$ could not be discriminated from the background even in the compilation.

## CONCLUSIONS

In summary, measurements of the force and blockade current characterizing the translocation of a *single* histone, impelled slowly and systematically through a sub-nanopore, exposed several interesting features that informed on the prospects for sequencing protein. The force measurements were interpreted to show that SDS used to stabilize denaturation was cleaved from the protein–SDS aggregate as it was impelled through the sub-nanopore. A dichotomy was observed in the translocation kinetics; the molecule either slid frictionlessly through the pore or it slipped-and-stuck. When the histone slid frictionlessly, nearly regular fluctuations were observed intermittently in the force and blockade current that were cross-correlated, with lags that corresponded to the separation between stretched AAs. Moreover, the amplitudes of the fluctuation in the blockade were well correlated with the occluded volume of AA quadromers in the protein sequence, but the imperfect read fidelity indicated a deficiency in the volume model for the blockade current. Regardless of the model, the difference in the patterns in the current fluctuations associated with the two practically identical histones supported the conclusion that a sub-nanopore was sensitive enough to discriminate AA substitutions in the sequence of *a single protein molecule* by measuring volumes of 0.1 nm$^3$ per read. Based on this evidence, it is speculated that the fluctuations observed in the differences reflect additional physical aspects of the histones not taken into account in the volume model such as hydration,[10,30,31] stiffness, mobility, or charge. Finally, importantly, a sub-nanopore was shown to be extraordinarily sensitive to residue substitutions in the protein sequence provided that the translocation was nearly frictionless, and the sensitivity improved with shrinking pore volume and slower translocation velocity.

## METHODS

**Sub-nanopore Fabrication.** As described elsewhere,[9] pores with sub-nanometer cross sections were sputtered through thin custom-made silicon nitride membranes (SiMPore, Inc. West Henrietta, NY) using a tightly focused, high-energy electron beam carrying a current ranging from 300 to 500 pA (postalignment) in a scanning transmission electron microscope (FEI Titan 80-300, Hillsboro, OR) with a Super-TWIN pole piece and a convergence angle of 10 mrad. For example, a 398 pA beam was used to sputter a nominally 0.3 nm diameter pore in 50 s. The silicon nitride was deposited by LPCVD directly on the top surface of a polished silicon handle wafer, and a membrane was revealed using an EDP (an aqueous solution of ethylene diamine and pyrocatechol) chemical etch through a window on the polished back-side of the handle. The thickness of the membranes, which ranged from $t = 9.3 \pm 0.9$ nm, was measured *in situ* using electron energy loss spectroscopy prior to sputtering. The roughness of the membrane, measured with custom-built silicon cantilevers (Bruker, Fremont, CA) with 2 nm radius tips, was estimated to be <0.5 nm rms.

**Multislice Image Simulations.** TEM images of the pores were simulated using the Dr. Probe software package described in detail elsewhere.[9,14] Tersely, the simulation procedure started by creating an atomistic model of the structure. An approximation to an amorphous $Si_3N_4$ membrane was created by randomly filling a tetragonal $5 \times 5 \times 10$ nm$^3$ ($x$–$y$–$z$) cell with Si and N atoms. The total number of atoms was determined by the volume (250 nm$^3$), the density of stoichiometric $Si_3N_4$ (3.44 g/cm$^3$), and the molecular weight of $Si_3N_4$ (140.28 g/mol). Atoms that were closer together than 0.16 nm were removed from the structure. In order to create a biconical pore with an elliptical cross section at the waist, atoms were selectively extracted from the volume within a border defined by the following mathematic model:

$$\sqrt{(x - 2.5 + c)^2 + (y - 2.5)^2} + \sqrt{(x - 2.5 - c)^2 + (y - 2.5)^2} = 2a$$



DOI: 10.1021/acsnano.6b08452
ACS Nano 2017, 11, 5440–5452

where $a = a_0 + \tan(\alpha)|z - 5|$, $b = b_0 + \tan(\alpha)|z - 5|$, and where $c = \sqrt{a^2 - b^2}$

$x$, $y$, and $z$ denote the coordinates of each atom (in nm), $\alpha$ is the cone angle, $a/b$ are the major and minor axes of the ellipse, and $c$ is the eccentricity.

The calculation of dynamic electron diffraction was performed using a multislice algorithm.[9,14] The input cells were partitioned into 40 equidistant slices along $z$. Phase gratings of the slices were then calculated on grids with 512 × 512 pixels in $x$ and $y$ for 300 keV incident electrons using the elastic and absorptive form factors and Debye−Waller factors to account for the thermal motion of the atoms. The multislice calculations yielded an exit-plane wave function consistent with the specified model of the structure. Based on the exit-plane wave functions, TEM images were constructed using a phase contrast transfer function consistent with the microscope and defocus, assuming instrumental parameters for the aberration coefficient ($C_s$ = 0.9 mm) and the aperture size of the objective (150 μm) at an acceleration voltage of 300 kV. Because the defocus was uncertain, a defocus series from −50 to 50 nm was calculated for comparison to the actual images. The TEM image calculations account for the partial temporal coherence with a focus spread of about 4 nm and for the partial spatial coherence with a 0.4 mrad semiangle of convergence.

**Preparation of Denatured Protein.** The biotinylated histones, H3.2 (#31271, Active Motif) and H3.3 (#31297, Active Motif), were purchased as lyophilized powders at a specified purity of ≥98% by SDS-PAGE, prior to biotinylation. A biotin tag was ligated to the N-terminus of H3.2, whereas H3.3 was biotinylated on the C-terminus. The purity of the H3.3 product was subsequently compromised because only 75% of the pure product was tagged with biotin, and so a portion of the pure product remained untagged. There were no other contaminants in the biotinylated H3.3 product, however. The untagged H3.3 was flushed away after tethering (see Force and Pore Current Spectroscopy with a Protein Tethered to an AFM).

These recombinant, carrier-free proteins were reconstituted according to the protocols offered by the manufacturer. Typically, the protein was reconstituted at high (25 μg/mL) concentration in phosphate buffered saline (PBS). Diluted with PBS (1 μg/mL), 100 μL aliquots were prepared from these solutions and mixed with 100 μL of 18 MΩ deionized water (DI), 0.5 mM β-mercaptoethanol (BME), and 0.05% (w/v) sodium dodecyl sulfate (SDS), vortexed, and heated to 85 °C for 2 h and allowed to cool to 20 °C. Subsequently, to ensure denaturation, circular dichroism (CD) spectra were acquired in the band between 195 and 260 nm. Whereas the CD spectra measured on the native protein showed evidence of an α-helix—two negative peaks near 208 and 222 nm,[32] no evidence of a remnant secondary structure was found after denaturation (Figure S3). The denatured SDS−protein aggregate was then either tethered to an AFM tip or added to the reservoir in the microfluidic device for data collection without a tether. When tethering to an AFM cantilever, aliquots of the stock solution were diluted again to 0.4 μg/mL using 1× PBS (see below).

Likewise, the control poly-L-lysine homopolymer with 100 repeated K residues (BT-PLK100, Alamanda Polymers), which was denoted as $K_{100}$, was biotinylated on the N-terminus and had a nonreactive alkylamide function on the C-terminus. Similarly, the other control poly-L-glutamic acid with 200 repeating E residues (BT-PLE200, Alamanda Polymers), denoted as $E_{200}$, was biotinylated on the C-terminus and had a nonreactive urea function on the N-terminus. Both were purchased as lyophilized powder at a purity of 90−100%. They were subsequently resuspended in 50 mL of 18 MΩ DI to form stock solutions of 2 mg/mL. Aliquots of these stock solutions were diluted 2000-fold with DI to produce 1 μg/mL for tethering. The same method was used to denature the homopolymers. For long-term storage, the solutions were kept in 1.5 mL centrifuge tubes at −80 °C to prevent degradation, whereas for short-term (day-to-day) use, they were stored at 4 °C.

**Microfluidic Fabrication.** The silicon chip supporting a single membrane with a single pore through it was bonded to a polydimethylsiloxane (PDMS, Sylgard 184, Dow Corning) microfluidic device formed using a mold-casting technique as described elsewhere.[15] The PDMS microfluidic was formed from a thoroughly stirred 10:1 mixture of elastomer (siloxane) with a curing agent (cross-linker) cast in a mold formed from DSM Somos ProtoTherm 12120 plastic (ProtoLabs, Raleigh, NC) and then degassed and cross-linked at 75 °C for 2 h. The microfluidic device consisted of two microchannels: one 250 × 75 $\mu m^2$ in the cross section on the *trans*-side and the other 8 mm in diameter on the *cis*-side connected by a *via* 500 μm diameter that contained the silicon chip supporting the silicon nitride membrane with a pore in it.

A tight seal was formed between the silicon chip and the PDMS *trans*-microfluidic channel with a plasma-bonding process. The membrane with a pore through it was plasma-bonded to the *cis*-side of the PDMS microfluidic using a (blue-white) 25 W oxygen plasma (PDS-001, Harrick Plasma, Ithaca, NY) for 30 s. The *cis*-channel was likewise sealed to a clean 75 × 25 $mm^2$ glass slide, 1 mm thick (VWR, Radnor, PA) using the same bonding strategy. To ensure a tight seal to the PDMS, the silicon nitride layer on top of the silicon chip was painted with PDMS, and then the ensemble was heat-treated at a temperature of 75 °C for 30−60 min. Separate Ag/AgCl electrodes (Warner Instruments, Hamden, CT) were embedded in the microfluidic to independently, electrically address the *cis*- and *trans*-sides of the membrane. Likewise, the two microfluidic channels were also connected to external pressure and fluid reservoirs through polyethylene tubing at the input and output ports. To remove trapped air, methanol was initially flowed through the microfluidic, and then immediately the channels were flushed and filled by 250 mM NaCl electrolyte. Subsequently, to wet the pore, an alternating voltage was applied for >1 day (typically). The *cis*-side was used to convey proteins to the pore via an AFM tip.

**Measurements of Current Blockades Due to Untethered Protein.** To measure the blockade current, a constant +0.70 V was applied to the anode on the *trans*-side of the membrane with the cathode on the *cis*-side grounded, and the corresponding pore current was measured in a Faraday cage at 22.7 ± 0.1 °C using an Axopatch 200B amplifier with the output digitized with the DigiData 1440 data acquisition system (DAQ, Molecular Devices, Sunnyvale, CA) at a sampling rate of 100−250 kHz. Clampex 10.2 (Molecular Devices, Sunnyvale, CA) software was used for data acquisition and analysis. To measure a blockade current, a bias was applied to the reservoir containing 200 μL of electrolytic solution containing $2 \times 10^{-4}$ % (w/v) SDS along with 300 pM of protein. Recombinant, carrier-free protein was reconstituted according to the protocols offered by the manufacturer. Typically, the protein was reconstituted at high (10 μg/mL) concentration in PBS without adding BSA to avoid false readings.

**Force and Pore Current Spectroscopy with a Protein Tethered to an AFM.** The force and current data were acquired from single protein molecules using a customized AFM (MFP-3D-BIO, Asylum Research, Santa Barbara, CA) interfaced to an inverted optical microscope (Axio-Observer Z1, Zeiss), all enclosed within a Faraday cage, as described elsewhere.[15] In particular, the low-noise Z-sensor in the AFM was coupled with an ultraquiet Z-drive to produce noise in the tip−sample distance <30 pm at 1 kHz bandwidth. To minimize drift and reduce acoustic noise, the inverted optical microscope was mounted on an optical air table with active piezoelectric vibration control (Stacis, TMC, Peabody, MA), housed in an acoustically isolated, NC-25 (noise criterion) rated room in which the temperature was stabilized to less than ±0.1 °C over 24 h through radiative cooling. Temperature fluctuations appeared to be the dominant source of long-term drift, and with temperature regulation, the drift of the system was reduced to 0.6 nm/min. Sound couples strongly into the microscope and was another potential source of instrument noise. Therefore, acoustically loud devices, especially those with cooling fans such as power supplies, amplifiers, and computers, were placed outside of the room. With these precautions, force detector noise is <10 pm/$\sqrt{Hz}$ for frequencies above 1 Hz; the on-surface positional noise measured <45 pm A-dev.

The Z-piezosensor (Z-sensor) was calibrated using a standard calibration grating (NT-MDT, Moscow, Russia). The deflection sensitivity was calibrated by pressing the tip against a freshly cleaved



DOI: 10.1021/acsnano.6b08452
ACS Nano 2017, 11, 5440−5452

mica surface and correlating the cantilever deflection to the Z-sensor reading. The spring constant was determined by measuring the thermal noise spectra and fitting the response to a simple harmonic oscillator.

To acquire the data, first, the topography of the silicon nitride membrane and the location of the pore relative to the edges of the membrane were determined in air in noncontact (tapping) mode using a silicon cantilever (SSS-FM, Nanosensors, Neuchatel, Switzerland) with a 2 nm nominal radius and a spring constant ranging from $K_{spr}$ = 0.5−9.5 nN/nm and a 45−115 kHz resonant frequency (in air). Force spectroscopy was performed in a 250 mM NaCl electrolytic solution, using a custom MSNL silicon cantilever (Bruker, Camarillo, CA) without metal reflex with a 2 nm tip radius. Each MSNL probe includes six cantilevers with a range of force constants ($10 < K_{spr} < 100$ pN/nm) and resonant frequencies ($7 < \omega_0 < 125$ kHz). Considering only the off-resonance thermal noise of the cantilever $\Delta F_{min} = \sqrt{4k_B T \Delta f K_{spr}/\omega_0 Q} < 1$ pN, where typically $K_{spr} \sim 10-30$ pN/nm, $\Delta f = 100-3300$ Hz was the measurement bandwidth, $\omega_0 = 2\pi \times 5.3-18$ kHz was the angular resonance frequency of the cantilever, and $Q \sim 15-17$ (0.8−1.3) was the quality factor in air (liquid).

To functionalize an AFM tip, the cantilever was first conditioned in a 20% oxygen plasma at 25 W (Harrick Plasma) for 1 min and then coated in a sealed container with 3-aminopropyltriethoxysilane (Gelest) by vapor deposition overnight. After this treatment, the cantilevers were stored at −20 °C for up to 10 days. Prior to a measurement, the cantilever was exposed to biotin-labeled BSA (1 μg/mL, A8549, Sigma-Aldrich) in a phosphate buffer saline solution (pH 7.4) for 45 min at 23 °C and rinsed with PBS and then placed in 100 μL of streptavidin (1 μg/mL, S4762, Sigma-Aldrich) in PBS for 45 min at 23 °C, rinsed in PBS, and finally immersed in denatured 30 nM protein (0.5 μg/mL) in PBS and incubated for another 45 min at 23 °C followed by a final rinse in 250 mM NaCl electrolyte before mounting on the cantilever holder. These rinses essentially removed extraneous material not bound by the streptavidin−biotin tether. The force on the frictionless plateaus and rupture forces associated with the "slip-stick" transitions were smaller than that required to rupture either the streptavidin−biotin or the nonspecific bond between BSA to silicon.[33]

To locate the pore relative to fiducial marks, that is, the edges of the ($4 \times 5$ μm$^2$) membrane, an AFM topographical scan was performed with a sharp tip in liquid in constant force (contact) mode. After that, the pore location was reacquired in liquid with a second cantilever on the same probe through triangulation from the fiducial marks and a small area scan. Then a constant +0.70 V was applied to the anode on the *trans*-side of the membrane with the cathode on the *cis*-side grounded, and the pore current was measured continuously with an external amplifier, whereas the force on the cantilever was determined from the deflection. Starting from a position about 100−120 nm above the membrane, the tethered protein, immersed in a solution of 250 mM NaCl electrolyte and SDS, was repeatedly advanced toward the sub-nanopore at 20 nm/s, captured, and threaded through it by the electric field and then retracted from it at a constant 4 nm/s velocity by the AFM while the current, tip deflection, and Z-position were recorded. The tip position above the membrane was determined from the sum of the tip deflection and Z-sensor position.

**Measurements of Current Blockades Due to a Protein Tethered to the AFM Tip.** The ionic current through a nanopore was measured in a Faraday cage with a patch-clamp amplifier (Axopatch 200B, Molecular Devices) in whole-cell mode. Ag/AgCl electrodes embedded in the microfluidic device were used to establish a transmembrane potential. An electrical bias of +0.70 V was applied between Ag/AgCl electrodes embedded in the *trans*- and *cis*-channels, and the current between them was measured using an Axopatch 200B amplifier at 17.6 ± 0.1 °C. Each data channel was subsequently digitally filtered at 5 kHz and sampled at 10 kHz and then digitally filtered again using a 100 Hz eight-pole Bessel filter (MATLAB, 2016a).

Protein adsorption was occasionally observed on the silicon nitride membrane (supplemental Figure S13).[34] To clear the membrane and reuse the pore, the microfluidic device was flushed with 18 MΩ DI for 2 days. Immersed in 250 mM NaCl, the open pore current noise with the AFM in place over the pore was about 16−22 pA rms at a 0.70 V bias for a 5 kHz bandwidth. The 40 Hz bandwidth used for a typical blockade current measurement reduced the rms noise to about 5−6 pA. To establish that it was clear of protein, the open pore current noise was evaluated again prior to an experiment. It was reused only if the current noise returned to that observed in the pristine pore. It was reused only if the current noise returned to that observed in the pristine pore. When a clog occurred, both the channel and reservoir were flushed with 18 MΩ DI; the reservoirs were then refilled with 250 mM NaCl electrolyte, and the polarity of the voltage imposed across the membrane was reversed to clear the pore. If this procedure failed to clear it, 0.01% (w/v) SDS solution was flushed through the channel to disperse latent aggregated protein in an attempt to recover the pore. In this way, sequencing data were acquired from one sub-nanopore for >28 days.

**Signal Autocorrelation Function.** Noise in the Z-positional sensor results in multiple measurements for each unique position. Thus, all time series were binned at unique Z-positions spaced every 25 pm, and the mean within each bin was calculated.[15] The spatial autocorrelation of the signal $S_z = \{S_1, S_2, ..., S_N\}$ at lag $k$ was calculated from $\mathrm{ACF}_k = \frac{1}{N}\sum_{z=1}^{N-k}(S_z - \bar{S})(S_{z+k} - \bar{S})$, where $\bar{S}$ represents the mean signal.

**Signal Estimation from Measurements of a Protein Tethered to the AFM.** The data handling has been described elsewhere.[9,15] Briefly, current blockades were manually cropped from the traces based on the start and end positions in time of a force plateau. The tip−surface distance was then estimated from the time stamp by summing the corresponding Z-sensor and cantilever deflection measurements. Fluctuations in the force and blockade current were identified and tallied. A threshold criterion of $2\sigma$ (two standard deviations) above the noise was employed to identify a fluctuation peak, and subsequently, an FIR digital Butterworth filter with a 40 Hz bandwidth was convolved with the data prior to cross-correlation.

Since they rarely spanned the entire molecule, single extractions had to be aligned before they were assembled into one "compilation". This alignment process required the determination of the start and end AAs associated with each blockade. Determining the "end" AA corresponding to the end of a blockade was trivial; it was simply the end of the molecule. For example, for a C-terminal cantilever tethered H3.3 molecule, the end of the blockade was associated with the free N-terminal of the chain. A small positional error (1 nm, <5%) on the end position was tolerated. To find the start position, the event length (in nm) was first divided by the AA periodicity observed in the current autocorrelation function. This value was then subtracted from the end point. Thus, a blockade 6 s long at a retraction velocity of 4 nm/s for which a 0.4 nm periodicity observed indicates that ($6 \times 4/0.4 =$) 60 AAs were retracted in totality during the blockade. Thus, the start point would be 60 AAs off from the molecular terminus. Once all events were assigned start and end points, they were normalized in current space so that every event contributed equally at each site to the final compilation. The average normalized current at each site was then found. Thus, in our figures, compilations of events are dimensionless to facilitate equal weighting of all events and optimal fitting to the volume model. In contrast, single events are represented in our graphs as current (pA).

The $r$ value, which is a measure of positional difference of force and current peaks, was calculated by subtracting each force and current peak position and taking the mean magnitude. The $p$ value represents the one-sided probability of observation of a given mean magnitude such that low values indicate an anomalously small difference in force and current peak positions. The $p$ values were calculated by setting up a Monte Carlo simulation of 1000000 force−current pairs (pseudoevents) exhibiting random but sequential peak placement of 20 AAs averaging 0.5 nm periodicity. The resulting distribution of 1000000 $r$ values was obtained by comparing current peak 1 to force peak 1, and so on. A fraction of these 1000000 pseudoevents exhibited



DOI: 10.1021/acsnano.6b08452
ACS Nano 2017, 11, 5440−5452

mean magnitudes less than a typical real event; this fraction is defined as $p$ value.

**Signal Estimation for Measurements of Untethered Protein.** Handling of untethered translocation data involved four steps, which were described in detail elsewhere:[9] (1) selection of blockades of sufficient duration from the raw current trace; (2) rescaling of blockades in time to the same number of data points and current level for averaging; (3) alignment of blockade translocation directions; and (4) renormalization of the consensus traces for comparison to the occluded volume model.

(1) Blockades were initially extracted from current traces recorded with a 10 kHz eight-pole Bessel filter using OpenNanopore but not always reliably.[35] Consequently, we resorted to custom MATLAB code. These codes allowed for the manual removal of multilevel events and open pore regions incorrectly categorized as true events. The settings for OpenNanopore were optimized by manual inspection of the open pore noise and the blockades. The magnitude of the blockade, $\Delta I$, local open pore current, $I_0$, and blockade duration, $\Delta t$, were calculated for each event. Events with sufficient duration to detect single AAs (assuming linear velocity) were selected according to the average number of intraevent peaks observed for a given protein, $C$, and the acquisition bandwidth cutoff, $D$ (*i.e.* $\tau > 2C/D$). Within this subset, blockades exhibiting a mean amplitude that was both five standard deviations ($5\sigma$) above the noise and within 10% of the mean expected percent blockade were selected.

(2) Assuming the peaks were periodic in time, all events were linearly resampled either into $N$ bins, where $N$ is the average number of peaks observed per event or 10 000 data points. For the purpose of averaging, all events were scaled to contribute equally to the final consensus traces.

(3) However, before averaging was performed, it was noted that blockades comprised two distinct groups, which showed similar peak maxima under temporal inversion. This observation was interpreted as evidence of two equivalent translocation directions, and so all events were sorted into two groups and the second was inverted in (normalized) time. The event blockades were then renormalized according to the median blockade percent and averaged.

(4) The model developed for the occluded volume shows variations in volume ($nm^3$) as a function of position. However, the events were recorded in units of pA. The scaling of pA to volume ($nm^3$) was necessary to compare the model and the consensus events, and can be directly inferred using both the pore geometry and open pore current. However, we chose to linearly scale the ordinate of the blockades to the volume model using a Nelder–Mead method search.

**Finite Element Simulations.** As described elsewhere, finite element simulations of vacated (open) pores, which ignored the atomistic details of the structure and electrolyte, were used to examine the distribution of the electrostatic potential and current.[9,15] Briefly, FESs of the electric field and the electro-osmotic flow were performed using COMSOL (v4.4, COMSOL Inc., Palo Alto, CA), following a Poisson–Boltzmann formalism described elsewhere. Briefly, the applied voltage $\varphi$ and the potential $\psi$ due to charges in the pore and on the protein are decoupled from one another and solved independently. The relationship between $\psi$ and the charge carriers, $Na^+$ and $Cl^-$, is given by the Poisson equation, $\nabla\psi = -\rho/\varepsilon\varepsilon_0$, where $\rho$, $\varepsilon$, and $\varepsilon_0$ are the volume charge density and the relative and vacuum permittivities, respectively. The charge density is given by $\rho = F\sum_i z_i c_i$, where $F$ = 96 485 C/mol is the Faraday constant, $z_i$ is the valence, and $c_i$ is the molar concentrations of ionic species $i$. The distribution of ions close to charged surfaces satisfies the Boltzmann distribution; thus, the charge density is given by $c_i = c_{0,i}\exp(-z_i e\psi/k_B T)$, where $c_0$ is the molar concentration (*i.e.*, bulk concentration), $e$ is the electric charge, $k_B = 1.38 \times 10^{-23}$ J/K is the Boltzmann constant, and $T$ = 298 K is the temperature.

Electro-osmotic flow was expressed by the Navier–Stokes equation, $\eta\nabla^2 u - \nabla p - F\sum_i z_i c_i \nabla V = 0$, where $V = \varphi + \psi$, $\eta$ is the viscosity, $p$ is the pressure, and $u$ is the velocity vector. The transport of ionic species is described by the Nernst–Planck equation given by $D_i\nabla^2 c_i + z_i\mu_i c_i \nabla^2 V = u\nabla c_i$, where $D_i$ is the diffusion coefficient and $\mu_i$ is the ionic mobility of the $i^{th}$ species. The parameters used in the simulations of ion transport in the pore volume such as the viscosity and diffusivity were tightly constrained by values gleaned from the literature (see supplemental Table S2).[36−42]

The electrophoretic force on a protein–SDS aggregate of radius $a$ and length $L_0$ with surface charge density $\sigma$ centered on a sub-nanopore was estimated using the axial component of the electric field $E_z = -\nabla V$ from $F_{eph} = 2\pi a\sigma\int_{-L_0/2}^{L_0/2} E_z(r = a,z)\mathrm{d}z$. The electro-osmotic force was given by $F_{eom} = 2\pi a\eta\int_{-L_0/2}^{L_0/2}\left.\frac{\mathrm{d}u_z(r,z)}{\mathrm{d}r}\right|_{r=a}\mathrm{d}z$, where $\eta$ is the viscosity and $u_z$ is the $z$-component of the velocity. The total net force was therefore $F_{eff} = F_{eph} - F_{eom}$.

## ASSOCIATED CONTENT

### Supporting Information

The Supporting Information is available free of charge on the ACS Publications website at DOI: 10.1021/acsnano.6b08452.

Tables S1 and S2, Figures S1–S13, and supplemental notes 1 and 2 (PDF)

Datafile containing tabulations of force and current measurements taken from six events (three H3.2 and three H3.3) that can be loaded into MATLAB (ZIP)

## AUTHOR INFORMATION


### Corresponding Author

*E-mail: gtimp@nd.edu.

### ORCID

Gregory Timp: 0000-0003-4418-5679


### Notes

The authors declare no competing financial interest.

## ACKNOWLEDGMENTS

This work was partially supported by a grant from the National Science Foundation [DBI 1256052], the Keough-Hesburgh Professorship, and the Walther Cancer Foundation.

## REFERENCES


(1) Laszlo, A. H.; Derrington, I. M.; Ross, B. C.; Brinkerhoff, H.; Adey, A.; Nova, I. C.; Craig, J. M.; Langford, K. W.; Samson, J. M.; Daza, R.; Doering, K.; Shendure, J.; Gundlach, J. H. Decoding Long Nanopore Sequencing Reads of Natural DNA. *Nat. Biotechnol.* **2014**, *32*, 829–833.

(2) Jain, M.; Fiddes, I. T.; Miga, K. H.; Olsen, H. E.; Paten, B.; Akeson, M. Improved Data Analysis for the MinION Nanopore Sequencer. *Nat. Methods* **2015**, *12*, 351–356.

(3) Clamer, M.; Höfler, L.; Mikhailova, E.; Viero, G.; Bayley, H. Detection of 3′-End RNA Uridylation with a Protein Nanopore. *ACS Nano* **2014**, *8*, 1364–1374.

(4) Edman, P.; Hogfeldt, E.; Sillen, L. G.; Kinell, P.-O. Method for Determination of the Amino Acid Sequence in Peptides. *Acta Chem. Scand.* **1950**, *4*, 283–293.

(5) Hughes, C.; Ma, B.; Lajoie, G. A. *De Novo* Sequencing Methods in Proteomics. *Methods Mol. Biol.* **2010**, *604*, 105–21.

(6) Armirotti, A.; Damonte, G. Achievements and Perspectives of Top-Down Proteomics. *Proteomics* **2010**, *10*, 3566–3576.

(7) Altelaar, A. F. M.; Munoz, J.; Heck, A. J. R. Next-Generation Proteomics: Towards an Integrative View of Proteome Dynamics. *Nat. Rev. Genet.* **2012**, *14*, 35–48.

(8) Brocchieri, L.; Karlin, S. Protein Length in Eukaryotic and Prokaryotic Proteomes. *Nucleic Acids Res.* **2005**, *33*, 3390–3400.

(9) Kennedy, E.; Dong, Z.; Tennant, C.; Timp, G. Reading the Primary Structure of a Protein with 0.07 $nm^3$ Resolution using a Sub-Nanometre-Diameter Pore. *Nat. Nanotechnol.* **2016**, *11*, 968–976.

(10) Kolmogorov, M.; Kennedy, E.; Dong, Z.; Timp, G.; Pevzner, P. Single-Molecule Protein Identification by Sub-Nanopore Sensors. *PLoS Comput. Biol.* **2017**, *13*, e1005356.




DOI: 10.1021/acsnano.6b08452
*ACS Nano* 2017, 11, 5440–5452

(11) Nakayama, J.-I.; Rice, J. C.; Strahl, B. D.; Allis, C. D.; Grewal, S. I. S. Role of Histone H3 Lysine 9 Methylation in Epigenetic Control of Heterochromatin Assembly. *Science* **2001**, *292*, 110−113.
(12) Saade, E.; Pirozhkova, I.; Aimbetov, R.; Lipinski, M.; Ogryzko, V. Molecular Turnover, the H3.3 Dilemma and Organismal Aging. *Aging Cell* **2015**, *14*, 322−333.
(13) Ho, C.; Qiao, R.; Heng, J. B.; Chatterjee, A.; Timp, R. J.; Aluru, N. R.; Timp, G. Electrolytic Transport through a Synthetic Nanometer-Diameter Pore. *Proc. Natl. Acad. Sci. U. S. A.* **2005**, *102*, 10445−10450.
(14) Barthel, J. *Dr. Probe-High-Resolution (S)TEM Image Simulation Software*, version 1.6, 2015, http://www.er-c.org/barthel/drprobe (accessed May 14, 2017).
(15) Nelson, E. M.; Li, H.; Timp, G. Direct, Concurrent Measurements of the Forces and Currents Affecting DNA in a Nanopore with Comparable Topography. *ACS Nano* **2014**, *8*, 5484−5493.
(16) Reynolds, J. A.; Tanford, C. Binding of Dodecyl Sulfate to Proteins at High Binding Ratios. Possible Implications for the State of Proteins in Biological Membranes. *Proc. Natl. Acad. Sci. U. S. A.* **1970**, *66*, 1002−1003.
(17) Gudiksen, K. L.; Gitlin, I.; Moustakas, D. T.; Whitesides, G. M. Increasing the Net Charge and Decreasing the Hydrophobicity of Bovine Carbonic Anhydrase Decreases the Rate of Denaturation with Sodium Dodecyl Sulfate. *Biophys. J.* **2006**, *91*, 298−310.
(18) Kozak, D.; Anderson, W.; Vogel, R.; Trau, M. Advances in Resistive Pulse Sensors: Devices Bridging the Void Between Molecular and Microscopic Detection. *Nano Today* **2011**, *6*, 531−545.
(19) Qin, Z. P.; Zhe, J. A.; Wang, G. X. Effects of Particle's Off-Axis Position, Shape, Orientation and Entry Position on Resistance Changes of Micro-Coulter Counting Devices. *Meas. Sci. Technol.* **2011**, *22*, 045804.
(20) Carrion-Vazquez, M.; Oberhauser, A. F.; Fowler, S. B.; Marszalek, P. E.; Broedel, S. E.; Clarke, J.; Fernandez, J. M. Mechanical and Chemical Unfolding of a Single Protein: a Comparison. *Proc. Natl. Acad. Sci. U. S. A.* **1999**, *96*, 3694−3699.
(21) Cheng, B.; Wu, S.; Liu, S.; Rodriguez-Aliaga, P.; Yu, J.; Cui, S. Protein Denaturation at a Single-Molecule Level: the Effect of Nonpolar Environments and its Implications on the Unfolding Mechanism by Proteases. *Nanoscale* **2015**, *7*, 2970−2977.
(22) Fluegel, S.; Fischer, K.; McDaniel, J.; Chilkoti, A.; Schmidt, M. Chain Stiffness of Elastin-Like Polypeptides. *Biomacromolecules* **2010**, *11*, 3216−3218.
(23) Lu, H.; Schulten, K. Steered Molecular Dynamics Simulation of Conformational Changes of Immunoglobulin Domain I27 Interpreted Atomic Force Microscopy Observations. *Chem. Phys.* **1999**, *247*, 141−153.
(24) Su, T.; Purohit, P. K. Mechanics of Forced Unfolding of Proteins. *Acta Biomater.* **2009**, *5*, 1855−1863.
(25) Małek, K. E.; Szoszkiewicz, R. Changes of Protein Stiffness During Folding Detect Protein Folding Intermediates. *J. Biol. Phys.* **2014**, *40*, 15−23.
(26) Wilson, J.; Sloman, L.; He, Z.; Aksimentiev, A. Graphene Nanopores for Protein Sequencing. *Adv. Funct. Mater.* **2016**, *26*, 4830−4838.
(27) Terwilliger, T. C. Rapid Model-Building of α-Helices in Electron Density Maps. *Acta Crystallogr., Sect. D: Biol. Crystallogr.* **2010**, *66*, 268−275.
(28) http://www.uniprot.org/uniprot/P84243 (H33_Human) (accessed May 14, 2017). http://www.uniprot.org/uniprot/Q71DI3 (H32_Human) (accessed May 14, 2017).
(29) Perkins, S. J. Protein Volumes and Hydration Effects. *Eur. J. Biochem.* **1986**, *157*, 169−180.
(30) Kyte, J.; Doolittle, R. A Simple Method for Displaying the Hydropathic Character of a Protein. *J. Mol. Biol.* **1982**, *157*, 105−132.
(31) Thanki, N.; Thornton, J. M.; Goodfellow, J. M. Distributions of Water around Amino Acid Residues in Proteins. *J. Mol. Biol.* **1988**, *202*, 637−657.
(32) Matsuo, K.; Yonehara, R.; Gekko, K. Secondary-Structure Analysis of Denatured Proteins by Vacuum-Ultraviolet Circular Dichroism Spectroscopy. *J. Biochem.* **2004**, *135*, 405−411.
(33) de Odrowaz Piramowicz, M.; Czuba, P.; Targosz, M.; Burda, K.; Szymonski, M. Dynamic Force Measurements of Avidin-Biotin and Streptavidin-Biotin Interactions Using AFM. *Acta Biochim. Polym.* **2006**, *53*, 93−100.
(34) Niedzwiecki, D. J.; Grazul, J.; Movileanu, L. Single-Molecule Observation of Protein Adsorption onto an Inorganic Surface. *J. Am. Chem. Soc.* **2010**, *132*, 10816−10822.
(35) Raillon, C.; Granjon, P.; Graf, M.; Steinbock, L. J.; Radenovic, A. Fast and Automatic Processing of Multi-Level events in Nanopore Translocation Experiments. *Nanoscale* **2012**, *4*, 4916−4924.
(36) Lynden-Bell, R. M.; Rasaiah, J. C. Mobility and Solvation of Ions in Channels. *J. Chem. Phys.* **1996**, *105*, 9266−9280.
(37) Xu, J. M.; Zou, X. Q.; Xie, Y. B.; Wang, Y. G. Molecular Dynamics Simulations on the Ionic Current through Charged Nanopores. *J. Phys. D: Appl. Phys.* **2009**, *42*, 105308.
(38) Zhou, J. D.; Cui, S. T.; Cochran, H. D. Molecular Simulation of Aqueous Electrolytes in Model Silica Nanochannels. *Mol. Phys.* **2003**, *101*, 1089−1094.
(39) Ortiz-Young, D.; Chiu, H. C.; Kim, S.; Voïtchovsky, K.; Riedo, E. The Interplay Between Apparent Viscosity and Wettability in Nanoconfined Water. *Nat. Commun.* **2013**, *4*, 2482.
(40) Li, T.-D.; Gao, J.; Szoszkiewicz, R.; Landman, U.; Riedo, E. Structured and Viscous Water in Sub-Nanometer Gaps. *Phys. Rev. B: Condens. Matter Mater. Phys.* **2007**, *75*, 115415.
(41) Goertz, M. P.; Houston, J. E.; Zhu, X.-Y. Hydrophilicity and the Viscosity of Interfacial Water. *Langmuir* **2007**, *23*, 5491−5497.
(42) Zhu, Y.; Granick, S. Viscosity of Interfacial Water. *Phys. Rev. Lett.* **2001**, *87*, 096104.



DOI: 10.1021/acsnano.6b08452
*ACS Nano* 2017, 11, 5440−5452